Journal of Materials Chemistry A

Accepted Manuscript

ROYAL SOCIETY OF CHEMISTRY

www.rsc.org/materialsA

Cite this: DOI: 10.1039/c0xx00000x

www.rsc.org/xxxxxx

ARTICLE TYPE

Enhancing the performance of Li_3VO_4 by combining nanotechnology and surface carbon coating for lithium ion batteries

Gaoqi Shao,[a] Lin Gan,[a] Ying Ma,[a] Huiqiao Li,*[a] and Tianyou Zhai*[a]

Received (in XXX, XXX) Xth XXXXXXXXX 20XX, Accepted Xth XXXXXXXXX 20XX

DOI: 10.1039/b000000x

With a large capacity and low voltage, Li_3VO_4 has recently attracted much attention as a new insertion-type anode material for lithium-ion battery. However, the poor electronic conductivity of Li_3VO_4 leads to large amount addition of inactive conduct agents in the electrode, which definitely sacrifices the electrode capacity and limits the rate performance. In this work, we propose a strategy in which Li_3VO_4 is first broken into nanometer scale by high energy ball milling to increase active surface and shorten the Li^+ diffusion distance, and then the particle surface is homogeneously coated with nanolayered carbon via a chemical vapor deposition (CVD) method for electronic conductivity enhancement. The obtained nanosized Li_3VO_4 is uniformly coated by ~ 5 nm carbon layers. Compared to untreated counterpart, the modified Li_3VO_4, attributed to the synergetic effects of nanosized and carbon coating, exhibits an increased first coulombic efficiency from 68.8% to 79.5%, a higher reversible capacity from 225 to 315 mAh g^{-1}, and superior rate performance. Importantly, the carbon-coated nanosized Li_3VO_4 with only 5% conductive additive exhibits better performances than the microsized raw Li_3VO_4 with 10% conductive additive, showing important effects of particle size and electronic conductivity on the electrochemical properties of Li_3VO_4.

Introduction

Lithium-ion batteries (LIBs), with the highest power and energy density among secondary batteries, are considered as the ideal powers for diverse applications from portable electronics to electric vehicles (EVs).[1] As an indispensable component of a battery, the anode material research has attracted much attention in recent years, resulted from the limitation faced by commercial graphite anode.[2,3] Many alternatives have been proposed to overcome the low capacity of graphite anode, in which the most known candidates are conversion type metal oxides and alloy-type Si/Sn-based alloys.[4-8] However, the conversion type anodes suffered a poor coulombic efficiency at the first cycle, and the alloy type materials suffered huge volume changes during charge/discharge.[7,8] Finally, the insertion-type material, such as graphite, is still proved to be the most practical anode for lithium ion batteries due to its good reversibility and high coulombic efficiency. Apart from graphite, $Li_4Ti_5O_{12}$ is another well-known insertion type anode material attracted the commercial interests.[9-12] $Li_4Ti_5O_{12}$ has a voltage plateau of 1.5V versus Li^+/Li and shows a zero volume effect during Li^+ intercalation, thus was used as a high safety and long life anode material. However, its excessive high voltage and low theoretical capacity (160 mAh g^{-1}) sacrifice the cell operation voltage and lead to a much lower energy density than graphite.

Recently, Li_3VO_4 rises as a new promising insertion type material. The structure of Li_3VO_4 is built up of oxygen atoms in approximately hexagonal close packing; the cations occupy ordered tetrahedral sites.[13] The octahedral sites are vacancy and connect to each other, established a three dimensional channel for lithium-ion diffusion. We first reported the electrochemical performances of Li_3VO_4 as an anode for LIBs and found Li_3VO_4 intercalates Li^+ at a lower voltage (0.5 ~ 1.0 V vs. Li^+/Li) than $Li_4Ti_5O_{12}$ and at the same time can deliver a specific capacity two times larger than that of $Li_4Ti_5O_{12}$.[14] Therefore, Li_3VO_4 promises a higher energy density than $Li_4Ti_5O_{12}$ as well as better safety than graphite. However, Li_3VO_4 undergoes a large voltage gap between its charge plateau and discharge plateau, a low initial coulombic efficiency, and poor rate capability, owing to its low electrode kinetics and poor electronic conductivity.[14] To enhance the lithium storage kinetics, decreasing the particle size to shorten the Li^+ diffusion length is a practical way, according to the formula of lithium diffusion time $\tau = L^2/2D$ where D is the diffusion coefficient, L is the diffusion length.[2,15,16] After the solid-state synthesis of Li_3VO_4, several solution-based approaches, such as hydrothermal treatment,[17,18] co-procipatation,[19] ultrasonic nebulization[20] and sol-gel approach,[21] were following developed electrochemical results showed that: compared with solid-state synthetic Li_3VO_4, the solution-based Li_3VO_4 exhibits a higher specific capacity due to their smaller particle size.

Li_3VO_4 is a fast Li-ion conductor but an electronic insulator.[22] The poor electronic conductivity severely affects the rate performances and leads to a large number addition of inactive conduct agents (>25 wt%) in the electrode, which definitely sacrifices the electrode capacity and limits the current efficiency. Surface carbon coating has been proved as an effective way to promote the electronic conductivity of electrode materials.[23,24] However, the high oxidation state of vanadium in Li_3VO_4 determines the synthesis of Li_3VO_4 preferring an air atmosphere. In such a condition, the carbon sources would be burnt out during the high temperature calcinations. An alternative way is to make a composite by post-dispersing carbon material into Li_3VO_4 or dispersing Li_3VO_4 into carbon material via a solution-based process. For example, Li *et al*[25] synthesized Li_3VO_4/CNT via a hydrothermal method and it exhibits excellent electrochemical property; Ni *et al*[26] deposited Li_3VO_4 on natural graphite via a quasi sol-gel method to fabricate a Li_3VO_4/graphite composite; Shi *et al*[27,28] and Jian *et al*[29] fabricated Li_3VO_4/graphene composites with enhanced cycle stability and rate performances due to the existence of high conductive graphene. Challenges of the post-adding carbon approach are that: the solution process is difficult to precisely control especially considering the diverse ionic forms of vanadium species; on the other hand, the post-added carbon is difficult to disperse homogeneously so that it cannot ensure an integrate coating of Li_3VO_4 surface. Up to now, the effective method to in-situ make a uniform and integrate surface coating of Li_3VO_4 with conductive material has not been developed yet.

Among the above-mentioned efforts, it can be noted that the previous way to modify Li_3VO_4 is either by "decreasing particle size" or "making composite with carbon" separately. In this work, we proposed a strategy to reduce the particle size of Li_3VO_4 together with homogeneously coating the particle surface by a nanolayer of conductive carbon. The nanosized Li_3VO_4 was prepared by simply high energy ball milling the solid-state synthesized product. Then it was surface coated by a chemical vapor deposition process. The existence of carbon coating layer can effectively prevent the particle growth at high temperature during carbon coating, thus nanosized carbon-coated Li_3VO_4 can be successfully obtained. Electrochemical performances show that the carbon-coated nanosized Li_3VO_4 with only 5% conductive additive can exhibit larger specific capacity, higher coulombic efficiency and better rate capability than those of the microsized raw Li_3VO_4 with 10% conductive additive.

Experimental Section

Sample preparation

Commercial V_2O_5 and Li_2CO_3 powder were firstly mixed in an agate mortar in a mol ratio of 1:3. The resultant mixture was heated at an air atmosphere at 600°C for 3h and then heated at 900°C for 3 h. The obtained pure phase Li_3VO_4 (denoted as Li_3VO_4-RAW) was ball milled in a ZrO_2 jar at a rotation speed of 350 rpm min^{-1} for 3 h using a high-energy ball milling machine (Fritsch, Pulverisett-6). The obtained nanosized Li_3VO_4 was denoted as Li_3VO_4-BM. After ball milling, the nanosized Li_3VO_4 was treated at 800°C for 2.5 h in a tube furnace where a toluene vapor was carried by N_2 gas though the reaction cube at a flow rate of 100 sccm. The obtained carbon-coated Li_3VO_4 was denoted as Li_3VO_4-BMC.

Material characterization

The morphology and microstructure of these samples were observed by scanning electron microscopy (SEM, FEI Sirion 200) and the high-resolution transmission electron microscopy (HRTEM, FEI Tecnai G2 F30). X-ray diffraction (XRD) data of these samples were recorded at room temperature with a PANalytical B.V. Empyrean diffractometer. Raman spectra were measured by a LabRAM HR800 spectrograph. Thermogravimetric (TG) of carbon coated Li_3VO_4 sample was tested under air at a heating rate of 10 °C min^{-1} with a PerkinElmer Instruments Pyrisl TGA. The surface state of these samples was investigated using X-ray photoelectron spectroscopy (XPS, Kratos AXIS-ULTRA DLD-600W).

Electrochemical measurements

Electrochemical measurements were performed using 2032 coin-type cells in which 1M $LiPF_6$ dissolved in the solution of ethylene carbonate (EC), dimethyl carbonate (DMC) and ethyl methyl carbonate (EMC) in 1:1:1 volume ratio was used as the electrolyte. The Li_3VO_4 electrodes were prepared by mixing 85% of active material, 10% of Super C_{45} and 5% of Polyvinylidene fluoride in weight except otherwise specified. The obtained slurries were covered on a copper foil and then dried in a vacuum oven at 80°C for 12h to remove the solvent before pressing. The electrode loading is ~ 5mg cm^{-2}. After drying and pressing, the electrode film was punched to disks of 10 mm in diameter for half cell tests. Charge/discharge measurements were carried between 3.0 V and 0.05 V with lithium metal as the other electrode on an automatic battery testing system of LAND CT2001A model.

Result and Discussion

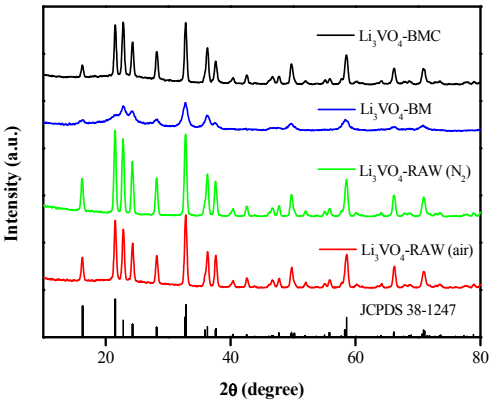

Figure. 1 XRD patterns of Li_3VO_4-RAW obtained by solid state reaction in air and N_2 atmosphere, Li_3VO_4-BM and Li_3VO_4-BMC.

Figure 1 shows XRD patterns of Li_3VO_4 obtained at different conditions, in which L_3VO_4-RAW (air) and Li_3VO_4-RAW (N_2) denote the raw material obtained by solid-state reaction in air and N_2 atmosphere, respectively; Li_3VO_4-BM denotes Li_3VO_4 raw product after treatment of high energy ball milling; Li_3VO_4-BMC

denotes Li_3VO_4 raw product after treatment of high energy ball milling and carbon coating. It can be seen that all the diffraction peaks of the four samples can be well indexed to the orthorhombic Li_3VO_4 phase (JCPDS No. 38-1247) with lattice parameters of a = 5.447 Å, b = 6.327 Å, c = 4.948 Å, and α = β = γ = 90°. Vanadium in Li_3VO_4 is in its highest valence, the absence of oxygen gas in the atmosphere during high temperature treatment (such as the process of carbon coating) may affect the phase purity of Li_3VO_4. Before carbon coating, we first check the product obtained by solid state reaction of Li_2CO_3 and V_2O_5 in N_2 atmosphere. XRD shows that Li_3VO_4-RAW (N_2) exhibits the same pattern as that of Li_3VO_4-RAW (air), indicating the formation of Li_3VO_4 phase is not so sensitive to oxygen. The result suggests the feasibility to perform CVD carbon coating on Li_3VO_4 under N_2 atmosphere. After high energy ball milling, the diffraction peaks of Li_3VO_4-BM are much broadened and the peak intensity is intensely decreased, which suggests a much reduced particle size and declined crystallization degree by ball milling. Further carbon coating the ball-milled sample via a CVD process at 800 °C for 2.5 h, the obtained Li_3VO_4-BMC sample shows sharp diffraction peaks again and the peak intensity also recovers to a high degree as Li_3VO_4-RAW sample. The phenomenon implies two possibilities: (1) the reduce-sized particle re-grows into larger sized particle during high temperature CVD process; (2) the deteriorated crystallization after ball milling is recovered by high temperature treatment. It is worthy to note that all the four samples show no impurity phases in their XRD patterns. Even at a high reductive atmosphere as the case of CVD carbon coating, Li_3VO_4 still maintains a high purity phase, indicating the outstanding chemical stability of Li_3VO_4. In the XRD pattern of Li_3VO_4-BMC, no signal of carbon is found, which is probably because the carbon content is too low to be detected. However, the sample colour was observed to change from white to black after carbon coating process, evidencing the mild carbon coating from the pyrolysis of toluene vapor.

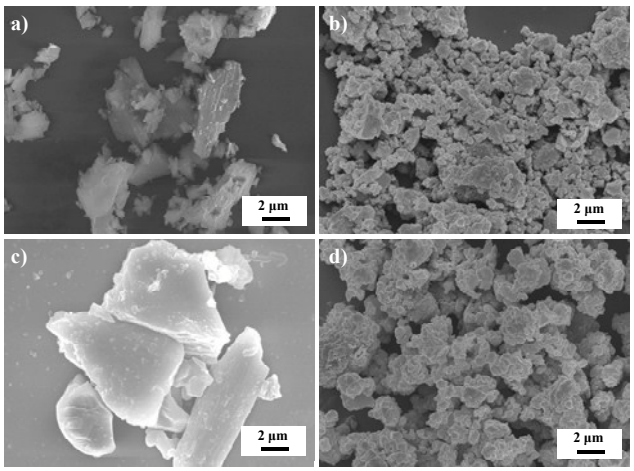

Figure. 2 SEM images of (a) Li_3VO_4-RAW by solid-state reaction; (b) Li_3VO_4-BM obtained by ball milling of Li_3VO_4-RAW; (c) Li_3VO_4-BM sample after treatment at 800 °C for 2.5 h with no presence of toluene vapor; (d) Li_3VO_4-BMC obtained by treatment of Li_3VO_4-BM at 800 °C for 2.5 h with presence of toluene vapor.

The morphology evolutions of Li_3VO_4 by treatment of ball milling and carbon coating were observed by SEM. As shown in Figure 2a, the Li_3VO_4-RAW sample by solid-state reaction consists of large irregular particles with size ranging from 3 to 8 μm. After high energy ball milling, the large particles are grinded into much smaller spherical particles of 300 ~ 500 nm in size, as shown by SEM of Li_3VO_4-BM in Figure 2b. This observation is consistent with the broadened XRD peaks of Li_3VO_4-BM in Figure 1. Carbon coating treatment was performed on Li_3VO_4-BM sample by thermo pyrolysis of toluene vapor at high temperature. To see the effect of such high temperature process on sample morphology, control experiments were carried out by treating Li_3VO_4-BM sample at same temperature for same time, with and without introducing carbon source vapor, respectively. Figure 2c shows the SEM image of Li_3VO_4-BM sample after annealing at 800 ℃ for 2.5 h without presence of toluene vapor. The nanosized spherical particles observed previously (Figure 2b) have grown completely up to large particles of tens of micrometers (Figure 2c). Such rapid growth of particle size suggests nanosized Li_3VO_4 is very sensitive to high temperature process. In contrast, with the presence of toluene vapor during high temperature treatment, Li_3VO_4-BMC sample (Figure 2d) maintains very well the nanoparticle morphology of its Li_3VO_4-BM precursor, which indicates the existence of carbon coating layer can effectively prevent the particle growth during annealing. At the same magnification, SEM image of Li_3VO_4-BMC shows more distinct particle edges than that of Li_3VO_4-BM, suggesting a higher conductivity of Li_3VO_4-BMC because of carbon coating. Associating the observation of SEM and XRD results, it is clear that the recovery of XRD peaks from Li_3VO_4-BM sample to Li_3VO_4-BMC sample is mainly attributed to the enhancement of crystallization degree by carbon coating process, rather than growth of particle size.

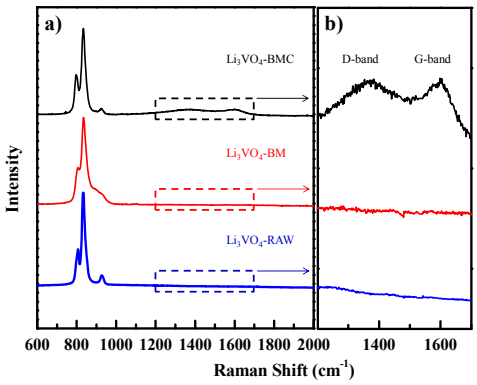

Figure. 3 Raman spectra of Li_3VO_4-RAW, Li_3VO_4-BM and Li_3VO_4-BMC.

Raman spectra (Figure 3) further confirm the existence of carbon in the samples after carbon coating. The three Raman peaks observed at ~ 807 cm^{-1}, ~ 834 cm^{-1} and ~ 927 cm^{-1} in Figure 3a are caused by vibrations of VO_4 tetrahedra, in good agreement with the typical Raman spectrum of Li_3VO_4.[30] For Li_3VO_4-RAW, the main peaks are strong and distinct. After ball-milling, the peaks at ~ 807 cm^{-1} and ~ 834 cm^{-1} for Li_3VO_4-BM become broader and the peak at ~ 927 cm^{-1} nearly disappears, due to the decreased crystallization. Further treating the ball milled sample by carbon coating at 800 °C for 2.5 h, both the peak width

and peak intensity of Li_3VO_4-BMC recover to the level of Li_3VO_4-RAW. The result indicates that the crystallization of Li_3VO_4 firstly decreased after ball-milling and then recovered after carbon-coating. The phenomenon is agree with the results of XRD. As is known, carbon materials usually exhibit two characteristic Raman peaks at ~ 1350 cm^{-1} and ~ 1580 cm^{-1}, which correspond to the D band of disordered carbon and G band of graphitized carbon, respectively. Figure 3b shows the magnified Raman spectra of the three samples in the range of 1200 ~ 1700 cm^{-1}. For Li_3VO_4-RAW and Li_3VO_4-BM, there is no peak found between 1200 ~ 1700 cm^{-1}. After carbon coating, Li_3VO_4-BMC shows two obvious Raman peaks at 1372 cm^{-1} and 1604 cm^{-1} respectively, which can be well indexed to the D band and G band of carbon.

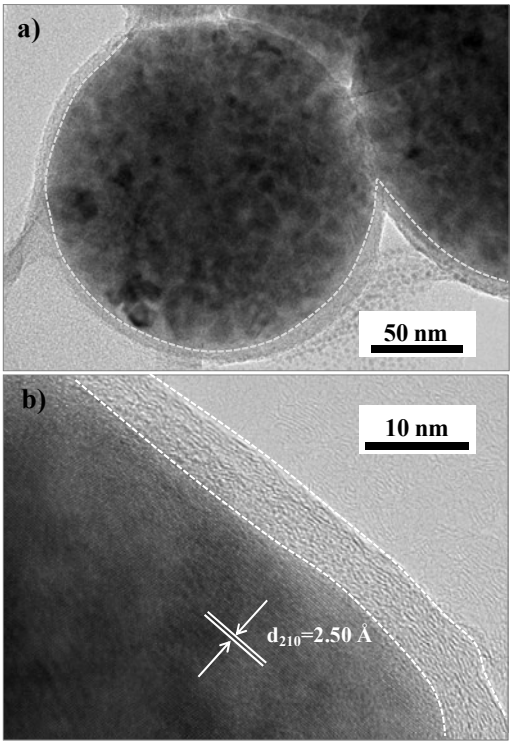

Figure. 4 HRTEM images of the carbon coated sample (Li_3VO_4-BMC).

Morphology details of the carbon coated sample (Li_3VO_4-BMC) were observed by TEM in Figure 4. The surface of the whole particle is fully coated by a uniform layer of carbon (Figure 4a), which ensures good conductivity along the particle boundaries and surrounding environment. The ordered lattice fringes of Li_3VO_4 can be clearly seen in Figure 4b, showing the high crystalline nature of Li_3VO_4-BMC sample, consistent with high resolution peaks in XRD and Raman. The interplanar crystal spacing is 2.50 Å, corresponding to the (210) plane of Li_3VO_4 (JCPDS 38-1247). At the edge of particle, a uniform carbon layer can be observed with a thickness of ~ 5 nm. The coated carbon layer is in semi-oriented lattice, indicating it is partially graphitized. Direct adding or mixing conductive carbon with Li_3VO_4 can also promote the electrode conductivity. However, it is difficult to achieve full conductive coating of Li_3VO_4. As a result, it requires a large amount of conductive agent to assure the electrode conductivity.[14, 25, 29] The unique feature of CVD method is that carbon sources are introduced in the form of vapor. It is very easy for a gas phase to access all solid surface, thus the deposited carbon would cover the entire solid surface and form a core-shell coating layer. On the other hand, the low carbon content in the source vapor facilitates a thin deposition layer of carbon. Such a full and thin coating of particle surface can make the best use of conductive carbon during the electrochemical processes.

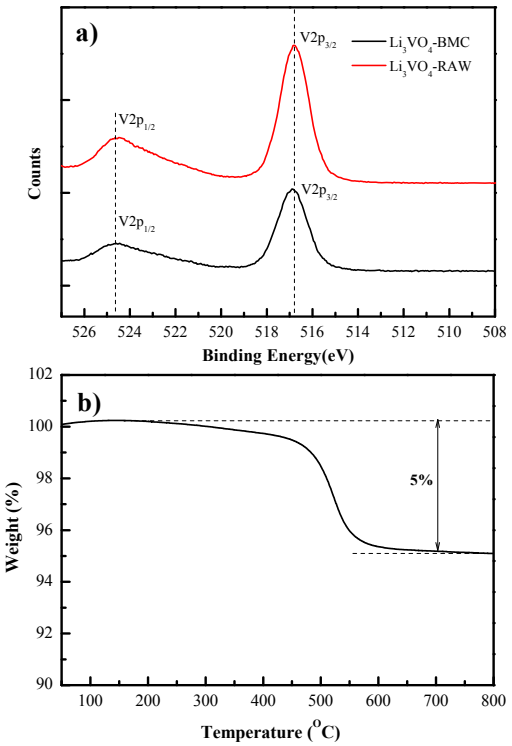

Figure. 5 (a) The V_{2p} core spectra of Li_3VO_4 before (RAW) and after carbon coating (BMC); (b) TG curve of Li_3VO_4-BMC measured from 40 °C to 1000 °C under an air flow of 60 mL min^{-1} with a heating rate of 10 °C min^{-1}.

During the process of CVD coating, the pyrolysis of toluene will produce elemental carbon and hydrogen, both of which are highly reductive especially at high temperature. XPS was carried out to analyze the surface state of Li_3VO_4 before and after carbon coating. In Figure 5a, two typical peaks at 524.6 eV and 516.9 eV can be observed in the V_{2p} core spectra, which are assigned to the $V_{2p1/2}$ and $V_{2p3/2}$ of V^{5+}, respectively. [31-33] The V_{2P} core spectra of Li_3VO_4-RAW and Li_3VO_4-BMC exhibit same peak profiles at same position, indicating the vanadium valence keeps in +5 before and after carbon coating. Combined with the results of XRD and Raman, it can be concluded that Li_3VO_4 can well maintain its structure, purity and valence in both cases of oxygen-deficient and high reductive atmosphere. In other words, the Li_3VO_4 phase possesses outstanding thermo-stability, thus can endure the highly reductive environment to achieve CVD carbon coating. Themogravimetry (TG) test was used to determine the carbon content in the coated sample. As shown in Figure 5b, the carbon content in Li_3VO_4-BMC is about 5% in weight.

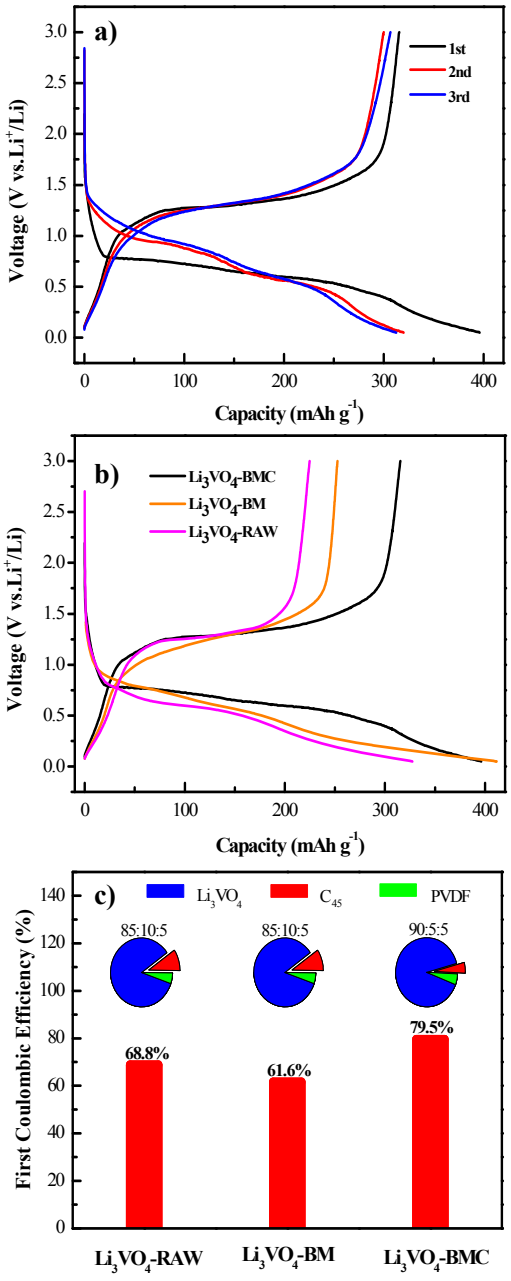

Figure. 6 (a) The first three cycles of galvanostatic discharge/charge curves of Li_3VO_4-BMC at a current density of 20 mA g^{-1} between 0.05 ~ 3.0 V versus Li^+/Li; (b) The initial discharge/charge curves of Li_3VO_4-RAW, Li_3VO_4-BM and Li_3VO_4-BMC at the current density of 20 mA g^{-1} between 0.05 ~ 3.0 V versus Li^+/Li; (c) The composition and first coulombic efficiency of Li_3VO_4-RAW, Li_3VO_4-BM and Li_3VO_4-BMC electrodes.

In electrochemical tests, the electrode of Li_3VO_4-RAW and Li_3VO_4-BM usually consist of 85% active material, 10% conductive agents and 5% binder. As determined by TG, the carbon content in L_3VO_4-BMC is about 5%. For convenience in comparison, the electrode of Li_3VO_4-BMC was made by 90% active material, 5% conductive agents and 5% binder. The specific capacity is calculated based on the weight of active material in the electrode. Figure 6a gives the first three cycles of galvanostatic discharge/charge curves of Li_3VO_4-BMC at a current density of 20 mAg^{-1} between 0.05 ~ 3.0 V versus Li^+/Li. It delivers a first discharge capacity of 396 mAh g^{-1} and a first charge capacity of 315 mAh g^{-1}, respectively, corresponding to a coulombic efficiency of 79.5%. There is little difference between the second and the third discharge/charge profiles, showing the electrode undergoes high reversible reactions after the first cycle. The initial discharge/charge curves of Li_3VO_4-RAW, Li_3VO_4-BM and Li_3VO_4-BMC are shown in Figure 6b and their first coulombic efficiencies are demonstrated in Figure 6c. The obtained first discharge/charge capacity for Li_3VO_4-RAW, Li_3VO_4-BM and Li_3VO_4-BMC is 327/225 mAh g^{-1}, 411/253 mAh g^{-1} and 396/315 mAh g^{-1}, respectively.

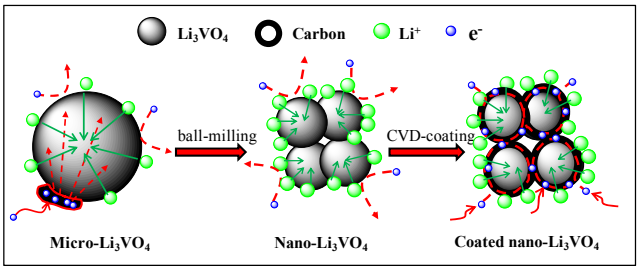

Figure. 7 The cases of lithium-ion diffusion and electron conduction in microsized Li_3VO_4, nanosized Li_3VO_4 and full carbon-coated nanosized Li_3VO_4. The green solid arrows and red dashed arrows illustrate the lithium-ion diffusion paths and electron conduction paths, respectively.

These observations can be interpreted by Figure 7. The large active particles of Li_3VO_4-RAW can only get electrons from the point-contacted carbon additive in the electrode due to the insulation of Li_3VO_4, thus the electron conduction in the particle is difficult and suffers a long conducting distance. Besides, such micro-particles hold both small reaction areas and long diffusion paths for Li^+ insertion. So, Li_3VO_4-RAW delivers the smallest charge/discharge capacity. After ball milling, the reduced particle size of Li_3VO_4 leads to a greatly-increased reaction surface for the insertion of Li^+, thus the reversible capacity (charge capacity) of Li_3VO_4-BM is larger than that of Li_3VO_4-RAW. For Li_3VO_4-BMC, both its reduced particle size and enhanced electronic conductivity by surface carbon coating can help to obtain high reaction activity for Li^+ insertion/de-insertion, thus delivering the largest reversible capacity among the three. Moreover, Li_3VO_4-BMC sample exhibits the highest coulombic efficiency of 79.5%, which is 17% and 10% larger than those of Li_3VO_4-BM (61.8%) and Li_3VO_4-RAW (68.8%), respectively. The irreversible capacity loss of Li_3VO_4 in the first charge/discharge process is mainly caused by the side reactions at the interface of electrode/electrolyte including formation of solid electrolyte interface (SEI) film and decomposition of electrolyte.[34,35] After fully coating the particle surface by carbon, the active Li_3VO_4 surface was protected by inert carbon layer, giving rise to a much stable carbon/electrolyte interface rather than Li_3VO_4/electrolyte interface. Therefore, Li_3VO_4-BMC sample accounts for a much enhanced current efficiency. In terms of Li_3VO_4-BM, its large area of uncoated surface is highly reactive for Li^+ insertion, but at the same time, for side reactions with electrolyte as well. As a result, it shows a higher capacity but lower current efficiency than raw Li_3VO_4 due to the increased side reactions at Li_3VO_4/electrolyte interface.

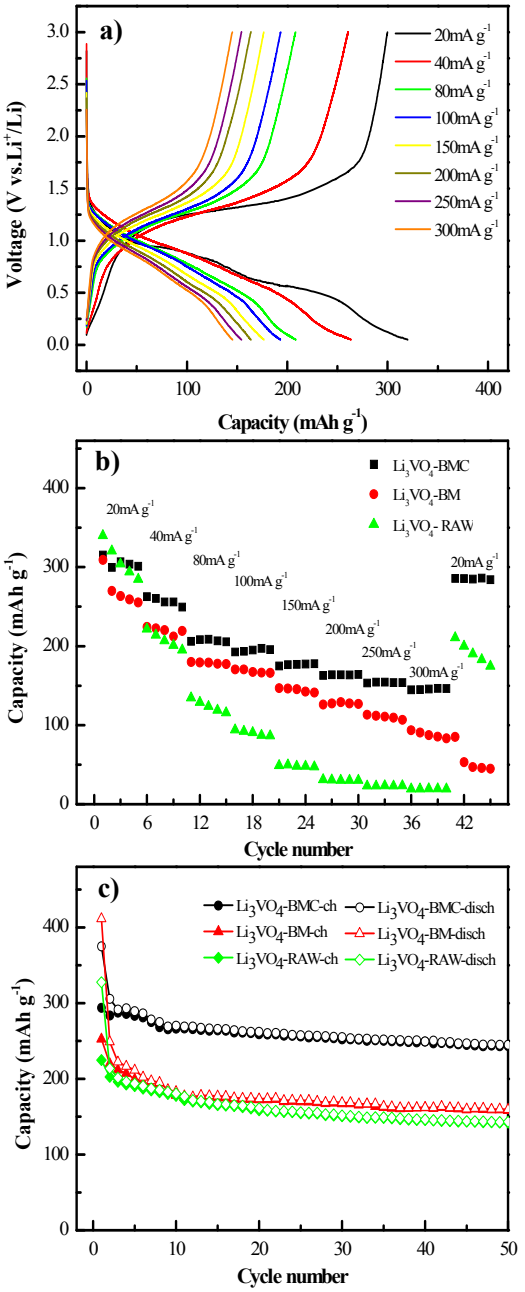

Figure. 8 (a) The charge and discharge profiles of Li_3VO_4-BMC at various current densities; (b) Rate performances of Li_3VO_4-RAW, Li_3VO_4-BM and Li_3VO_4-BMC at different current densities; (c) Cycle performances of Li_3VO_4-RAW, Li_3VO_4-BM and Li_3VO_4-BMC at constant current of 20 mA g^{-1} between 0.05 ~ 3.0 V versus Li^+/Li.

The electronic conductivity of electrode material will greatly affect its fast charge-discharge performance. Here, we use coin–type cells (2032) to evaluate the rate performances of different Li_3VO_4 samples. All the coin cells were tested between 0.05 ~ 3.0 V vs. Li^+/Li. The typical charge and discharge profiles of Li_3VO_4-BMC at various current densities were shown in Figure 8a. With the increase of current density, the obtained reversible discharge capacity of Li_3VO_4-BMC gradually decreases from 320 mAh g^{-1} at 20 mA g^{-1} to 193 mAh g^{-1} at 100 mA g^{-1} and 147 mAh g^{-1} at 300 mA g^{-1}. When the current density is returned to 20 mA g^{-1}, the discharge capacity recovers to 288 mAh g^{-1}, much close to the initial capacity, as shown in Figure 8b. The rate performances of Li_3VO_4-RAW and Li_3VO_4-BM are also given in Figure 8b. In contrast, the capacity of Li_3VO_4-BM decreased rapidly at elevated current density. Even the current goes back to 20 mA g^{-1}, the capacity doesn't recover to its original level, indicating the capacity loss of Li_3VO_4-BM at high current rates is irreversible. For Li_3VO_4-RAW, without ball milling and carbon coating, it delivers the fastest capacity decay at increased current rates. As shown in Figure 7, the microsized particles of Li_3VO_4-RAW account for not only poor electrical conductivity but also long diffusion paths for lithium-ions, both of which would lead to slow electrode kinetics and in turn poor rate performances. After ball-milling, the significantly decreased particle size can shorten the Li^+ diffusion paths, thus Li_3VO_4-BM sample shows better rate performance than Li_3VO_4-RAW of large particles. Combined nanosized particles and full surface coating of conductive carbon, Li_3VO_4-BMC sample promises both shortened Li^+ diffusion paths and fast electronic conductivity along all particle surfaces and boundaries, so it delivers the most enhanced high rate charge/discharge properties. For example, the capacity of Li_3VO_4-RAW, Li_3VO_4-BM and Li_3VO_4-BMC is found to be 17 mAh g^{-1}, 85 mAh g^{-1} and 147 mAh g^{-1} at the same current density of 300 mA g^{-1}, respectively. What should be noted is that the conductive agent in Li_3VO_4-BMC electrode is only 5% in weight, much lower than those in previously reports on Li_3VO_4 where 20 wt% ~ 30 wt% conductive materials were contained in Li_3VO_4 electrode.[14,25,29] The low amount of conductive additive in an electrode is important for the practical application since it can help to obtain a higher tap density and larger electrode capacity. With only 5% conductive additive, Li_3VO_4-BMC sample still shows very good rate capability, showing the great effects of nanolayered carbon coating. After 50 cycles of charge/discharge at a constant current of 20 mA g^{-1}, Li_3VO_4-BMC sample can maintain a specific capacity of 245 mAh g^{-1} with a coulombic efficiency of nearly 100%, as shown in Figure 8c. In contrast, the capacity of Li_3VO_4-RAW sample has decayed to 143 mAh g^{-1} after 50 cycles charge and discharge. It can be found the cycle performance of Li_3VO_4-BM is similar to that of Li_3VO_4-RAW, which may be the trade off between increased capacity and deteriorated dissolution of active material in the case of reduced particle size. For Li_3VO_4-BMC, its surface carbon coating layer, derived from hydrolysis of toluene, possesses high chemical stability. The coating layer can protect the core Li_3VO_4 particle from corrosion and dissolution in electrolyte. Therefore, Li_3VO_4-BMC exhibits a good cycle performance with high coulombic efficiency.

Conclusions

In summary, we developed a facile and effective way to obtain full carbon-coated nanosized Li_3VO_4 by combining ball-milling and CVD method. Nanosized particles can shorten the Li-ion diffusion path and increase the activity of Li_3VO_4, thus ball-milled Li_3VO_4 in nanosized shows increased specific capacity and improved rate performance compared to those of raw Li_3VO_4 in microsize. However, the reduced particle size gives rise to a larger area of directly contact between Li_3VO_4 and electrolyte,

leading to deteriorate coulombic efficiency at the first cycle. Through a CVD process in mixed atmosphere of N_2 and toluene, the surface of Li_3VO_4 can be uniformly and fully coated by a nanolayer of semi-graphitized carbon. The vanadium valence of Li_3VO_4 was found to maintain at +5 after carbon coating, showing its outstanding stability in even high reductive atmosphere. The presence of carbon coating layer can greatly improve the electronic conductivity of Li_3VO_4, prevent Li_3VO_4 from corrosion and dissolution in electrolyte, and decrease the side reactions at electrode/electrolyte interface during charge/discharge. Thus, carbon-coated nanosized Li_3VO_4 exhibits much enhanced electrochemical performances. At a very low content of conductive additive (5%), it exhibits a superior rate capability, stable cycle performance and larger specific capacity with a much promoted first coulombic efficiency than those of raw Li_3VO_4. The results indicate that combination of nanotechnology and surface carbon coating is an effective way to enhance the electrochemical performances of Li_3VO_4 anode material.

Acknowledgements

We acknowledge the support from National Nature Science Foundation of China (51302099, 21322106, 51472097), Ministry of Science and Technology of China (2015CB932600), Program for New Century Excellent Talents in University (NCET-13-0227) and National 1000 Young Talents Program of China. We thank the Analytical and Testing Center of Huazhong University of Science and Technology.

Notes and references

[a] *State Key Laboratory of Materials Processing and Die & Mould Technology, School of Materials Science and Engineering, Huazhong University of Science and Technology, Wuhan 430074, P. R. China. E-mail: hqli@hust.edu.cn; zhaity@hust.edu.cn*

1. L. Li, Z. Wu, S. Yuan, X. B. Zhang, *Energy Environ. Sci*., 2014, **7**, 101.
2. P. G. Bruce, B. Scrosati, J. M. Tarascon, *Angew. Chem. Int. Ed.,* 2008, **47**, 2930.
3. M. G. Kim, J. Cho, *Adv. Funct. Mater*., 2009, **19**, 1497.
4. X. L. Huang, R. Z. Wang, D. Xu, Z. L. Wang, H. G. Wang, J. J. Xu, Z. Wu, Q. C. Liu, Y. Zhang, X. B. Zhang, *Adv. Funct. Mater.*, 2013, **23**, 4274.
5. D. L. Ma, Z. Y. Cao, H. G. Wang, X. L. Huang, L. M. Wang, X. B. Zhang, *Energy Environ. Sci.,* 2012, **5**, 8538.
6. C. Z. Yuan, H. B. Wu, Y. Xie, X. W. Lou, *Angew. Chem. Int. Ed.,* 2014, **53**, 1488.
7. R. Malini, U. uma, T. Sheela, M. Ganesan, N. G. Renganathan, *Ionics,* 2009, **15**, 301.
8. H. K. Liu, Z. P. Guo, J. Z. Wang, K. Konstantinov, *J. Mater. Chem.,* 2010, **20**, 10055.
9. M. M. Rahman, J. Z. Wang, M. F. Hassan, D. Wexler, H. K. Liu, *Adv. Energy Mater.*, 2011, **1**, 212.
10. H. G. Jung, S. T. Myung, C. S. Yoon, S. B. Son, K. H. Oh, K. Amine, B. Scrosati, Y. K. Sun, *Energy Environ. Sci.*, 2011, **4**, 1345.
11. L. Zhao, Y. S. Hu, H. Li, Z. X. Wang, L. Q. Chen, *Adv. Mater.*, 2011, **23**, 1385.
12. K. S. Park, A. Benayad, D. J. Kang, S. G. Doo, *J. Am. Chem. Soc*., 2008, **130**, 14930.
13. A. R. West, F. P. Glasser, *J. Solid State Chem.*, 1972, **4**, 20.
14. H. Q. Li, X. Z. Liu, T. Y. Zhai, D. Li, H. S. Zhou, *Adv. Energy Mater*., 2013, **3**, 428.
15. C. Wu, F. Feng, Y. Xie, *Chem. Soc. Rev*., 2013, **42**, 5157.
16. H. Q. Li, P. He, Y. G. Wang, E. Hosono, H. S. Zhou, *J. Mater.Chem*., 2011, **21**, 10999.
17. S. B. Ni, X. H. Lv, J. J. Ma, X. L. Yang, L. L. Zhang, *J. Power Sources*, 2014, **248**, 122.
18. S. B. Ni, X. H. Lv, J. J. Ma, X. L. Yang, L. L. Zhang, *Electrochim. Acta*, 2014, **130**, 800.
19. W. T. Kim, Y. U. Jeong, Y. J. Lee, Y. J. Kim, J. H. Song, *J. Power Sources*, 2013, **244**, 557.
20. W. T. Kim, B. K. Min, H. C. Choi, Y. J. Lee, Y. U. Jeong, *J. Electrochem. Soc.,* 2014, **161**, A1302.
21. Z. Y. Liang, Y. M. Zhao, L. Z. Ouyang, Y. Z. Dong, Q. Kuang, X. H. Lin, X. D. Liu, D. L. Yan, *J. Power Sources,* 2014, **252**, 244.
22. A. Khorassani, A. R. West, *J. Solid State Chem.*, 1984, **53**, 369.
23. H. Q. Li, H. S. Zhou, *Chem. Commun.*, 2012, **48**, 1201.
24. X. Wang, X. Q. Cao, L. Bourgeios, H. Guan, S. M. Chen, Y. T. Zhong, D. M. Tang, H. Q. Li, T. Y. Zhai, L. Li, Y. Bando, D. Golberg, *Adv. Funct. Mater.*, 2012, **22**, 2682.
25. Q. D. Li, J. Z. Sheng, Q. L. Wei, Q. Y. An, X. J. Wei, P. F. Zhang, L. Q. Mai, *Nanoscale*, 2014, **6**, 11072.
26. S. B. Ni, X. H. Lv, J. C. Zhang, J. J. Ma, X. L. Yang, L. L. Zhang, *Electrochim. Acta*, 2014, **145**, 327.
27. Y. Shi, J. Z. Wang, S. L. Chou, D. Wexler, H. J. Li, K. Ozawa, H. K. Liu, Y. P. Wu, *Nano Lett.*, 2013, **13**, 4715.
28. Y. Shi, J. Cao, H. D. Abruna, H. J. Li, H. K. Liu, D. Wexler, J. Z. Wang, Y. P. Wu, *Chem. Eur. J.*, 2014, **20**, 5608.
29. Z. L. Jian, M. B. Zheng, Y. L. Liang, X. X. Zhang, S. Gheytani, Y. C. Lan, Y. Shi, Y. Yao, *Chem. Commun.*, 2015, **51**, 229.
30. V. Massarotti, D. Capsoni, M. Bini, P. Mustarelli, G. Chiodelli, C. B. Azzoni, P. Galinetto, M. C. Mozzati, *J. Phys. Chem. B*, 2005, **109**, 14845.
31. J. Mendialdua, R. Casanova, Y. Barbaux, *J. Electron Spectrosc. Relat.Phenom.*, 1995, **71**, 249
32. N. Alov, D. Kutsko, I. Spirovova, Z. Bastl. *Sur. Sci.*, 2006, **600**, 1628.
33. H. Q. Li, T. Y. Zhai, P. He, Y. G. Wang, E. Hosono, H. S. Zhou, *J. Mater. Chem.*, 2011, **21**, 1780.
34. J. H Song, H. J. Park, K. J. Kim, Y. N. Jo, J. S. Kim, Y. U. Jeong, Y. J. Kim, *J. Power Sources*, 2010, **195**, 6156.
35. A. R. Armstrong, C. Lyness, P. M. Panchmatia, M. S. Islam, P. G. Bruce, *Nat. Mater.*, 2011, **10**, 223.